PROCEEDINGS, 43rd Workshop on Geothermal Reservoir Engineering
Stanford University, Stanford, California, February 12-14, 2018
SGP-TR-213

Quantifying EGS Permeability Development Using Induced Seismicity

Jeremy Riffault, David Dempsey, Rosalind Archer and Satish Karra

Department of Engineering Science, University of Auckland Private Bag 92019 Auckland 1142, New Zealand

jrif565@aucklanduni.ac.nz

Keywords: EGS, stimulation, induced seismicity, Habanero, permeability

ABSTRACT

In Enhanced Geothermal System (EGS) projects, high pressure injection of cold water is conducted with the aim to artificially enhance in-situ permeability. Assessing the spatial distribution of this permeability enhancement is critical in an EGS setting, as it indicates the success of these stimulation operations, and gives valuable information for future development of the project. Such stimulations typically induce large seismicity clouds, the origin of those micro-earthquakes being mainly attributed to sliding along preexisting cracks caused by pore pressure increase. Therefore, the distribution and intensity of the microseismicity cloud makes it possible to track fluid pressure evolution, which in turn reveals aspects of the permeability distribution and its enhancement.

Using this idea, we develop a method to invert permeability development based on the distribution of seismicity in a 2D plane, allowing for simulation of non-azimuthal symmetry. We design a permeability assignment model where each node has its own semi-independent permeability regime. The density of earthquake hypocenters is derived from the pressure distribution obtained from a flow simulator. An inverse problem is set up in which a synthetic permeability enhancement regime is created and which we then attempt to recover from simulated microseismicity, accounting for both location and Poisson errors.

While the inversion successfully recovers much of the true permeability regime, we find that the inclusion of post-stimulation seismicity is critical to constrain hydrological conditions in the final moments of the stimulation. We also note that the presence of uncertainties in the earthquake observations leads to a discrepancy between the best fitted model and the real parameter set the parameter set; the range of valid solutions should be chosen carefully. Overall the proposed method is able to constrain the spatial distribution of permeability enhancement.

1. INTRODUCTION

During the 2003 Habanero#1 stimulation, in South Australia, 20,000 m^3 of water were injected into granitic basement at a depth of 4.25 km with the goal of creating an enhanced geothermal reservoir (Baisch et al., 2006). To assess the success of this operation, two sets of data are available: injection parameters (Figure 1), and a microseismicity catalog comprising 10,436 located microearthquakes (MEQs) (Figure 2). From these data, we seek to develop a method that can derive the where and at what rate permeability around the well was enhanced.

Injectivity, the ratio of injection flow rate to wellhead pressure, gives an estimate of the timing of permeability enhancement. During the Habanero stimulation, for the first two constant-rate injection steps, injectivity decreased with time, as is expected in the case that no permeability or porosity changes are occurring. However, from the third step, injectivity stabilizes and stays constant even though injection is continued at higher flow rates. This suggests that some permeability enhancement is occurring in such a way that the ability of the formation to take fluid remains constant in spite the increasing amount of fluid injected. However, injection parameters on their own do not uniquely constrain the spatial distribution of the permeability evolution.

A microseismicity catalog is composed of a list of MEQs, each attached to a location and an occurrence time. Its spatiotemporal nature makes it a valuable information source to study the stimulation process. For example, during the Habanero stimulation, it was noticed that the cloud developed with a planar shape (Figure 2), suggesting the existence of a planar structure directing the spread of the injected fluid. Indeed, induced seismicity is usually attributed to hydroshearing, the shear failure of existing fractures as a result of fluid pressure increase (Pearson, 1981). Moreover, as the same process can potentially increase permeability through the created mismatch between the two surfaces of the sheared fracture, the idea that the seismically active volume is representative of the stimulated volume has been popularized (Weidler et al., 2002). However, at least in Habanero, this does not seem to be the case, as there was a considerable amount of seismicity registered during the first two steps of injection (Figure 2), whereas injectivity evolution did not indicate any significant permeability enhancement (Figure 1).

But if seismic triggering is primarily an indicator of pressure increase, this means that it is possible to recover the spatiotemporal distribution of fluid overpressure. From the pressure distribution, we can invert the permeability distribution. This idea has been already investigated by several research groups. In Shapiro et al. (2005) the rate at which induced seismicity spreads away from a wellbore is used to obtain hydrological properties of the reservoir. In Tarrahi and Jafarpour (2012) a method is presented to invert rock permeability

distribution from the distribution of the microseismicity cloud using the ensemble Kalman filter. To our knowledge, this method was not applied to a permeability distribution evolving in time. The dataset of the 2003 Habanero stimulation was used in Dempsey et al. (2016), where a high permeability structure around the well was revealed from the distribution of the induced seismicity cloud.

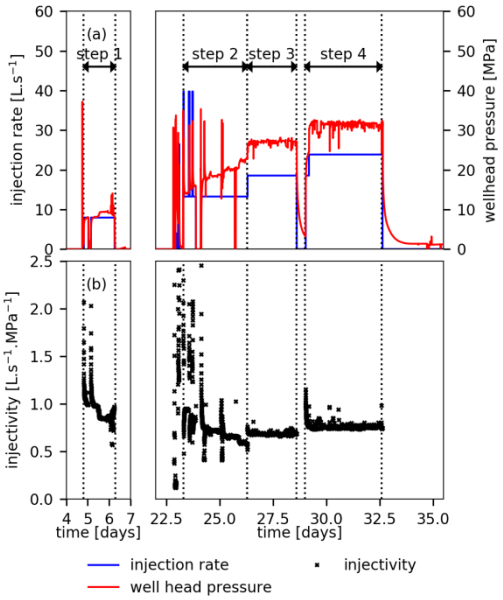

Figure 1: Injection parameters for the 2003 Habanero stimulation

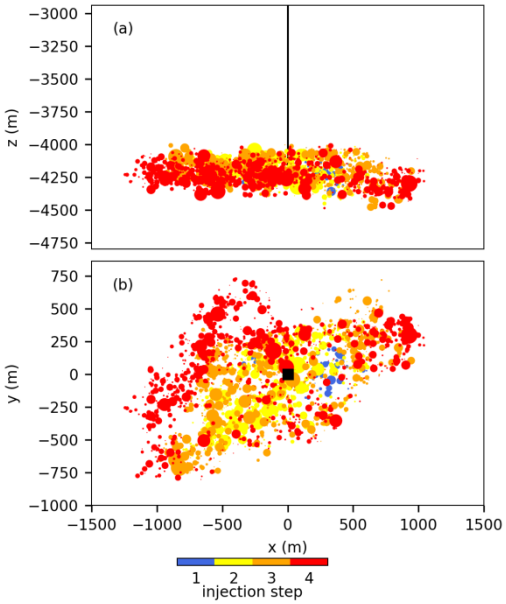

Figure 2: Induced seismicity distribution recorded during the 2003 Habanero stimulation

Similarly, in this paper we use the induced seismicity distribution as a proxy for pore pressure, enabling us to recover permeability changes. A first version of the method presented here was developed for the 2011 Paralana stimulation (Riffault et al., *submitted*). In that study, a 1D radial model was assumed, whereas here we generalize the study to handle 2D planar models. This is in an attempt to capture azimuthal asymmetry in the reservoir development. From Riffault et al. (*submitted*), it was concluded that, for the Paralana stimulation, permeability enhancement was limited to volumes immediately adjacent to the wellbore, and that the stimulated volume represented only a small fraction of the seismically active volume.

Here, we wish to demonstrate the feasibility of a 2D permeability enhancement inversion. First we detail the simulation workflow, from the permeability assignment model to the generation of seismicity. Then we set up an inversion problem that attempts to recover a

synthetic permeability evolution regime from pressure and seismicity observations alone. Observation errors are simulated and accounted for by the workflow. The goal is to develop a proof of concept, identify possible pitfalls and failures of the method, before it is applied to real dataset. As such, a simple model is used with a fewer number of nodes and parameters than intended for real-world applications.

2. TWO DIMENSIONAL MODEL

We model the propagation of injected fluid within a 2D injection plane. In contrast to other approaches, permeability at every discretized node and every time step is prescribed, rather than a function of the simulation variables (e.g., temperature, pressure or stress). The intent is that our inversion will reveal the spatiotemporal nature of permeability enhancement unconstrained by modeler bias in regards to the physical mechanisms.

Fluid flow and heat transfer during injection of cold water are modelled in the reservoir simulator FEHM (Zyvoloski 2007), which uses the control volume method. We use a simple 7x7 node grid, where each node is associated with a 200x200x20 m^3 volume (Figure 3). Injection occurs in the center node at a constant flow rate of 1.2 $kg.s^{-1}$ and a temperature of 100°C, in a reservoir at 60 MPa and 220°C, similar to the conditions found at the Habanero EGS site (Baisch et al. 2006). The injection lasts for 24 hours.

2.1 Permeability Model Construction

There are an infinite number of possibilities for constructing a permeability evolution scenario. We introduce several constraints that, while not strictly always correct, nevertheless seem reasonable simplifications: (i) at all times during the stimulation, permeability should be higher the closer one is to the injection node; and (ii) as few parameters as possible should be employed. These restrictions lead to a much simpler inversion process. Indeed, without the first constraint, permeability at the edges of the model would be much harder to recover, as it has almost no impact on the way in which fluid spreads throughout the domain.

We use a simple model where permeability, κ_i, at node, i, and time t, is given by:

$$\kappa_i(t) = \begin{cases} \kappa_{0,i}, & t \le t_i \\ \kappa_{0,i} + \dfrac{t - t_i}{t_{\max} - t_i}\left(\kappa_{1,i} - \kappa_{0,i}\right), & t > t_i \end{cases} \tag{1}$$

where $\kappa_{0,i}$, $\kappa_{1,i}$, t_i, t_{max} are, respectively, initial permeability, final permeability, time of first permeability enhancement, and simulation end time. We assume an isotropic permeability. Here, κ always refer to the logarithm in base 10 of the permeability in m^2. For each node, i, the three parameters can be different, and the permeability evolution scenario of the whole model is described by the matrix $\boldsymbol{\kappa}$:

$$\boldsymbol{\kappa} = \begin{bmatrix} \kappa_{0,1} & \kappa_{1,1} & t_1 \\ \vdots & \vdots & \vdots \\ \kappa_{0,N_{nodes}} & \kappa_{1,N_{nodes}} & t_{N_{nodes}} \end{bmatrix} \qquad \mathrm{R}^{\cdot\cdot_{nodes}\times 3} \tag{2}$$

where N_{nodes} is the number of nodes in the model. However, the components of $\boldsymbol{\kappa}$ are not independent, because of our self-imposed condition that permeability must always be higher nearer to the wellbore. To make sure this condition is respected, we design a system where each node, i, has a rank, R_i, attached as presented on Figure 3. Ranks are used to direct the sequence by which local permeability parameters are assigned. Before presenting the permeability assignment method, we first require the definition of two sets of parameters on which $\boldsymbol{\kappa}$ depends: $\boldsymbol{\Theta} = \left[\kappa_{0,min}, \kappa_{0,max}, d\kappa, t_\kappa\right]$, which bounds the values of $\boldsymbol{\kappa}$ over the whole model, and

$$\boldsymbol{\Psi} = \begin{bmatrix} \alpha_1 & \beta_1 & \gamma_1 \\ \vdots & \vdots & \vdots \\ \alpha_{N_{nodes}-1} & \beta_{N_{nodes}-1} & \gamma_{N_{nodes}-1} \end{bmatrix} \qquad 1]^{(N_{nodes}-1)\times 3} \tag{3}$$

which controls permeability interdependencies between neighboring nodes. For $R = 0$, at the injection node, we define $\kappa_{0,i} = \kappa_{0,max}, \kappa_{1,i} = \kappa_{0,max} + d\kappa, t_i = t_\kappa$. This explains why $\boldsymbol{\psi}$ is of dimension $\left(N_{nodes} - 1\right)\times 3$ and not $N_{nodes}\times 3$ as $\boldsymbol{\kappa}$ is, because for the injection node the permeability parameters do not depend on $\boldsymbol{\psi}$. For $R > 0$, considering the directly neighboring node with the highest $\kappa_{0,j}$, j, we have:

$$\begin{aligned}\kappa_{0,i} &= \alpha_i \left(\kappa_{0,j} - \kappa_{0,min}\right) + \kappa_{0,min} \\ \kappa_{1,i} &= \beta_i \left(\kappa_{1,j} - \kappa_{0,i}\right) + \kappa_{0,i} \\ t_i &= \gamma_i \left(t_j - t_{\max}\right) + t_{\max}\end{aligned} \tag{4}$$

Thus the dependency of $\boldsymbol{\kappa}$ with $\boldsymbol{\Theta}$ and $\boldsymbol{\psi}$ is complete, and our self-imposed constraint dictating that permeability will always be higher as we get closer to the injection node is respected.

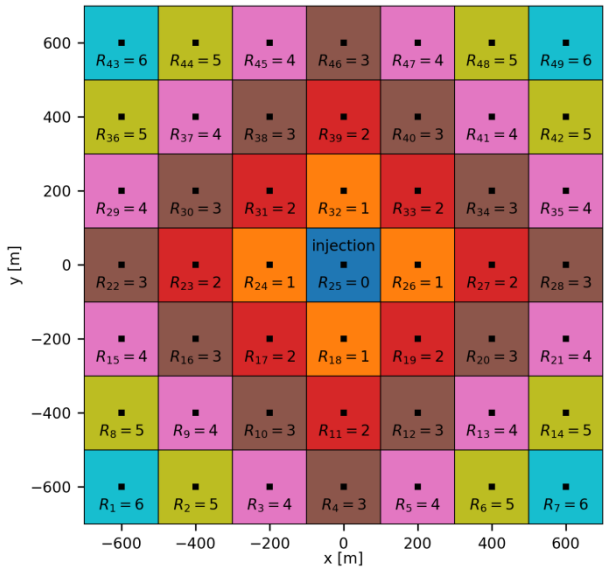

Figure 3: 2D model sketch and ranks, *R*, used for permeability assignment model.

Inevitably, the design of our permeability model introduces some bias. Permeability will tend to converge quickly towards $\kappa_{0,min}$ at the boundaries of the domain. Also, the rank system prevents certain patterns from appearing, such as larger permeability further away from the wellbore than closer, or convoluted permeability evolution scenarios. However, this design can be viewed as a regularization term: we expect permeability in the volumes close to the wellbore to reach higher values than further away. This design is a reasonable tradeoff that allows us to reduce the number of possible permeability models, thereby increasing the efficiency of the inversion process.

2.2 Injection Pressure and Hypocenter Density

With the permeability evolving as prescribed by $\boldsymbol{\Theta}$ and $\boldsymbol{\psi}$, the pressure, P, at the injection node is simulated at every time step. To simulate induced seismicity, we first need to define a meaningful measure of seismic activity, accounting for its discrete and aleatoric nature. Instead of considering each event independently, we compute the cumulative number of events within volumes, averaging over the heterogeneities. Following Dempsey et al., 2016, we obtain the spatiotemporal distribution of hypocenter density, n, defined as the total number of earthquake hypocenters occurring per unit of area of the injection plane prior to time, t. Its calculation is detailed in Section 3.1. This variable has been shown in Dempsey et al., 2016 to be a good proxy for pore pressure changes, thus able to reveal underlying physical changes responsible for seismicity triggering.

With our simulation, we obtain the pressure difference ΔP_i caused by the injected fluid at every node and every time step. The assumptions that hypocenter density and pressure difference follow a linear relationship allow us to estimate the number of earthquakes generated in the volumes associated to each of those nodes. For this, an additional parameter set is required, $\boldsymbol{\Phi} = \left[k, \Delta P_{crit}\right]$.

$$n_i(t) = \begin{cases} 0, & \Delta P_i \le \Delta P_{crit} \\ k\Delta P_i, & \Delta P_i > \Delta P_{crit} \end{cases} \tag{5}$$

We assume that k and ΔP_{crit} are constant over the spatial domain considered. However, we should also account for the Kaiser effect, which suggests that the cumulative hypocenter density depends on the maximum pressure change observed in the volume associated with node, i, at any precedent time (Baisch et al., 2006). Thus, Equation 5 becomes:

$$n_i(t) = \begin{cases} 0, & \max\left[\Delta P_i\left(t_0,..,t\right)\right] \le \Delta P_{crit} \\ k\left(\max\left[\Delta P_i\left(t_0..t\right)\right] - \Delta P_{crit}\right), & \max\left[\Delta P_i\left(t_0,..,t\right)\right] > \Delta P_{crit} \end{cases} \quad (6)$$

where t_0 is the starting time of the simulation. Thus we obtain n, the hypocenter density values, at every time step and every node. Both n and P are functions of the parameter vector $\mathbf{\Omega} = \left[\mathbf{\Theta}, \mathrm{vec}\left(\mathbf{\Psi}\right), \mathbf{\Phi}\right]$, and their computation is an entirely deterministic process.

3. INVERSION METHOD

Here, we define a set of true permeability parameters and use this as an input to our simulation framework to obtain pressure and induced seismicity distributions. This becomes a synthetic dataset. Then, we attempt to recover the true parameters using only the synthetic data, accounting for the impact of simulated uncertainties in the observations. Through integration of those simulated uncertainties, we produce the observations, different from the synthetic dataset. We wish to understand if the inversion procedure can successfully recover a sufficient range of permeability regimes that a good enough fit to the synthetic observations is achieved. Throughout this section, we will use the following nomenclature, with the example of the hypocenter density distribution, where $\overline{n}$, $\tilde{n}$, n^*, $[n]$, n_{min}, n_{max} are, respectively, the synthetic dataset, the observations, the best-fit (maximum likelihood) values obtained through inversion, the ensemble obtained from inversion satisfying a goodness of fit criterion, the minimum, and maximum values for the ensemble. While n^* (and P^*) are associated with a set of parameters, $\mathbf{\Omega}^*$, n_{min} and n_{max} are not. Instead, they regroup the extreme value of the ensemble of parameters [$\mathbf{\Omega}$]. Similarly, $\mathbf{\Omega}_{min}$ and $\mathbf{\Omega}_{max}$ are not elements of [$\mathbf{\Omega}$], they are its extreme values for each component.

3.1 Synthetic Data

According to our permeability model, we choose the true values $\overline{\mathbf{\Omega}}$ for our synthetic model. $\overline{\mathbf{\Theta}}$ and $\overline{\mathbf{\Phi}}$ values are given in Table 1.

Table 1: parameter values of Θ and Φ for the synthetic dataset and prior distribution

Parameters	True value	Minimum value	Maximum value
Minimum initial permeability, $\kappa_{0,min}$ [log(m^2)]	-16	-17	-15
Maximum initial permeability, $\kappa_{0,max}$ [log(m^2)]	-14	-15	-13
Permeability change, $d\kappa$ [log(m^2)]	2.0	1	3
Time of permeability enhancement start, t_κ [days]	0.5	0	1
Proportionality factor for MEQs triggering, k, [MEQs km^{-2} MPa^{-1}]	200	0	400
Critical pressure change, ΔP_{crit} [MPa]	0.2	0	0.4

The values of $\overline{\mathbf{\Psi}}$ are generated randomly, considering a uniform permeability distribution between 0 and 1 for each component. Using our simulator, we obtain $\overline{n}$ and $\overline{p}$. In a real life situation, while we can obtain reliable measurement of pressure changes at the injector, hypocenter density distribution is trickier. To emulate a real dataset, we generate a catalog of events using $\overline{n}$ and from it derive an observed hypocenter density distribution, $\tilde{n}$. In this process, we include a location and Poisson error, which means that $\overline{n} \neq \tilde{n}$. The Poisson distribution models the intrinsic aleatoric component of earthquake triggering (Langenbruch et al. 2011). We generate a number of MEQs $N_{MEQ,i}$ at a node, i, at time $t+dt$ following a Poisson process, according to:

$$N_{MEQ,i}\left(t+dt\right) = Poisson\left(\max\left[n_i\left(t+dt\right) - \sum_{t_0}^{t} N_{MEQ,i}(t)\right]\right) \quad (7)$$

For each MEQ, a time is assigned randomly following a uniform distribution in $[t, t+dt]$. Spatially, each MEQ is assigned a position randomly following a uniform distribution within the volume associated with the node, i. In addition, a normal distribution of mean, μ =

0 and standard deviation, σ_r, is used to represent the location error, which is added along both the x and y axis. As for the other parameters, σ_r is considered constant within the studied domain. Thus we obtain a list of earthquakes, with each event being associated a time and location within the plane of injection. This simulates the MEQ catalog that would be recorded for a certain permeability evolution scenario, incorporating both location and Poisson uncertainty. The value of k was selected in order to obtain a similar number of MEQs in our catalog as observed in Habanero, 10,436. The location error σ_r is the same as the relative location error in Habanero, 2 m.

Now, effort must be made to recover a hypocenter density temporal and spatial distribution based on this catalog. The first step is to assign for each event m the probability to be within a bin, i, of surface, S, in order to consider location uncertainty. For an event with position $\left[x_m, y_m\right]$, its probability to be within the bin i is p_m. Considering the bin delimited along the x axis by $\left[x_0, x_1\right]$, the component of p_m along the same axis, $p_{x,m}$ is:

$$p_{x,m} = \int_{x_0}^{x_1} \frac{1}{\sqrt{2\pi\sigma_r^2}} e^{-\frac{(x-x_m)^2}{2\sigma_r^2}} dx = \frac{1}{2}\left[\mathrm{erf}\left(\frac{x_1 - x_m}{\sigma_r\sqrt{2}} \right) - \mathrm{erf}\left(\frac{x_0 - x_m}{\sigma_r\sqrt{2}} \right) \right] \tag{8}$$

$p_{y,m}$ is calculated in the same way, and thus we have $p_m = p_{x,m} \times p_{y,m}$. At a specific time, t when N_t events occurred in total, in a bin, i, we have a Poisson binomial distribution, where each event, m has a probability, p_m of occurring in this bin. The probability of $j=0,..,N_t$ events to have occurred in the bin, i at the time, t is $P_t(k=j)$. The mean of this distribution is $\mu_l = \sum_1^{N_t} p_m$, and its variance is $\sigma_l^2 = \sum_1^{N_t} (1 - p_m)\, p_m$. Location uncertainty is thus considered, but not Poisson uncertainty. Indeed, when we generate our earthquake catalog, a Poisson distribution is introduced to simulate the random nature of earthquakes, and this must be taken in account when reconstructing the hypocenter density distribution. For each j in $0,..,N_t$ we consider a Poisson distribution weighted by $P_t(k=j)$. We obtain a new, larger distribution, and, when dividing by the area of the bin, i, is centered on $\tilde{i}$ and has a standard deviation of $\tilde{\sigma}$. Thus from $\bar{n}$ we obtain $\tilde{i}$ and $\tilde{\sigma}$. This is a stochastic process, for which each realization will give a different outcome. While $\bar{n}$ is the hypocenter density distribution which reflects the set of parameter $\bar{\Omega}$, $\tilde{i}$ does not accurately, as it is skewed by the inclusion of uncertainties.

3.2 Genetic algorithm

Because of the large number of parameters, a genetic algorithm is chosen for the inversion process (Schmitt, 2001). A population of individuals, each defined by its genotype, $\mathbf{\Omega}$, is evolved toward a better solution. All parameters are normalized in the [0, 1] interval. The evaluation of the fitness of each individual is done through the calculation of an objective function, $\theta(\mathbf{\Omega})$. We add the square difference for injection pressure with the Chi-square misfit for hypocenter density:

$$\theta(\mathbf{\Omega}) = \sum\left(\tilde{i} \quad \text{-} \quad \right)^2 + w\sum \frac{1}{\tilde{\sigma}} \left(\tilde{i} \right)^2 \tag{9}$$

where w is a weight arbitrarily set to ensure a good balance between the fit to wellbore pressure and the fit to the hypocenter density distribution. Our investigations shows w=2 to provides satisfying performance, considering our number of observation points. Because $\bar{n} \neq \tilde{i}$, the objective function $\bar{\theta} = \theta\left(\bar{\mathbf{\Omega}}\right)$ is not null, we find $\bar{\theta}$ = 0.23.

The inversion is an iterative process, with the population of each iteration called a generation. To form a new generation, a set of individuals from the previous generation is selected stochastically based on their fitness, and their genotype are mutated and recombined. We used a two points crossover as our recombination methods, with each pair of individuals having a 50% chance to generate an offspring in this fashion. To mutate genotypes, each individual has a 20% chance of seeing a random normal distribution of mean σ = 0 and standard deviation (the mutation rate) μ = 0.02 applied to its genotype. We make sure that parameters stay within their [0, 1] bounds.

The mutation rate is the only parameter where some experimental variation is conducted. While a larger mutation rate gives a faster convergence for models far from the global optimum, convergence is much slower as we get closer to the optimum. The mutation rate also impacts how far from the located best fit the parameter ensemble spreads, as with a smaller mutation rate the parameter range will

be much more concentrated around the minimum. The mutation rate is thus important to balance in order to obtain quick convergence and an ensemble of parameters of a satisfying size.

For a 49 node model, we have 150 parameters in **Ω**. For our initial population of 400 individuals, each individual had its parameters assigned randomly according to a uniform distribution, in [0, 1] for **ψ**, and within the bounds provided in Table 1 for **Θ** and **Φ**. Our goal is not only to find the global optimum, but also to find a range of possible parameter sets [**Ω**] with a good enough fit, with the real parameter set $\overline{\mathbf{\Omega}}$ included within this range. We arbitrarily set the goodness of fit criterion as models for which $\theta < 2\theta^*$.

4. RESULTS

For this inversion, 2600 generations are computed. The minimum objective function value obtained, θ^*=0.18, is less that for $\overline{\theta}$ (Figure 4). The inversion converges to a set of parameter which gives a better fit to the observations than a model with the real set of parameter, because it attempts to recreate the hypocenter density distribution $\tilde{\imath}$ instead of $\overline{n}$. Accordingly, the difference between $\tilde{\imath}$ and n^* is almost always smaller than the difference between $\tilde{\imath}$ and $\overline{n}$ (Figure 6). This is a good demonstration that the parameter vector which gives the best fit in a calibration is not a sufficient result, as it will always be different from the true parameters. For pressure, we do not have such concerns, as we assume $\overline{P} = \tilde{\imath}$, or that perfect measurement is possible, and the fit is quite satisfying (Figure 5).

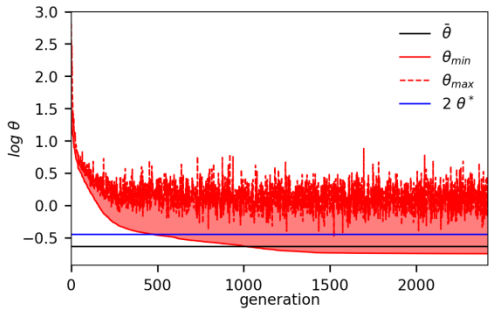

Figure 4:Objective function ensemble (pink) values for each generation over the course of the inversion.

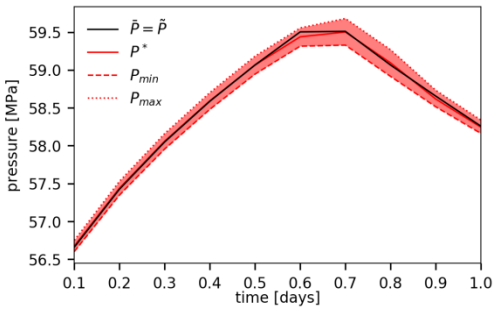

Figure 5: Pressure evolution with time for synthetic data and inverted set of parameters.

With $\theta^* > 0$, the fit is not perfect. However, as $\tilde{\imath}$ is derived from $\overline{n}$ with the inclusions of uncertainties, we do not know if a set of parameter **Ω** exists which would produce a perfect fit to $\tilde{\imath}$ and $\tilde{\imath}$. Thus we cannot be certain to have found the global optimum in the parameter space studied.

For our criterion of "good enough" fitting parameter sets, we obtain 364,671 models with $\theta < 2\theta^* = 0.36$. Because $\bar{\theta}$ is inferior to $2\theta^*$, if the parameter ensemble is complete, $\overline{\mathbf{\Omega}}$ should be within [**Ω**], and thus each of its values should be within $\mathbf{\Omega}_{min}$ and $\mathbf{\Omega}_{max}$. This is the case for **ψ**, and even with the inclusion of Poisson and location uncertainties, both k and ΔP_{crit} are well constrained by the inversion (Figure 8). For the permeability scaling parameter vector **Θ**, this is not true for three of the four parameters. However, because of the large number of permeability parameters and our complex permeability assignment model, it is more than likely that there is a lot of overlap between parameter impacts on the diffusion regime. Indeed, even with an ensemble of 364,671 models, this is not enough to discover every possible combination of the 146 parameters that result in similar permeability evolution scenarios. To better study the inclusion of the true parameters in the ensemble, it is more judicious to look at the permeability values at different times at each node. We find that $\overline{\kappa}$ is always included within κ_{min} and κ_{max} during most of the simulation, with the exception of t=1 day. Final simulation time aside, because the permeability difference between κ_{min} and κ_{max} is relatively small, we conclude that the inversion has converged

towards a single permeability enhancement regime, with multiple scenarios possible representing small variations of this regime. The true scenario is also a variation of this regime.

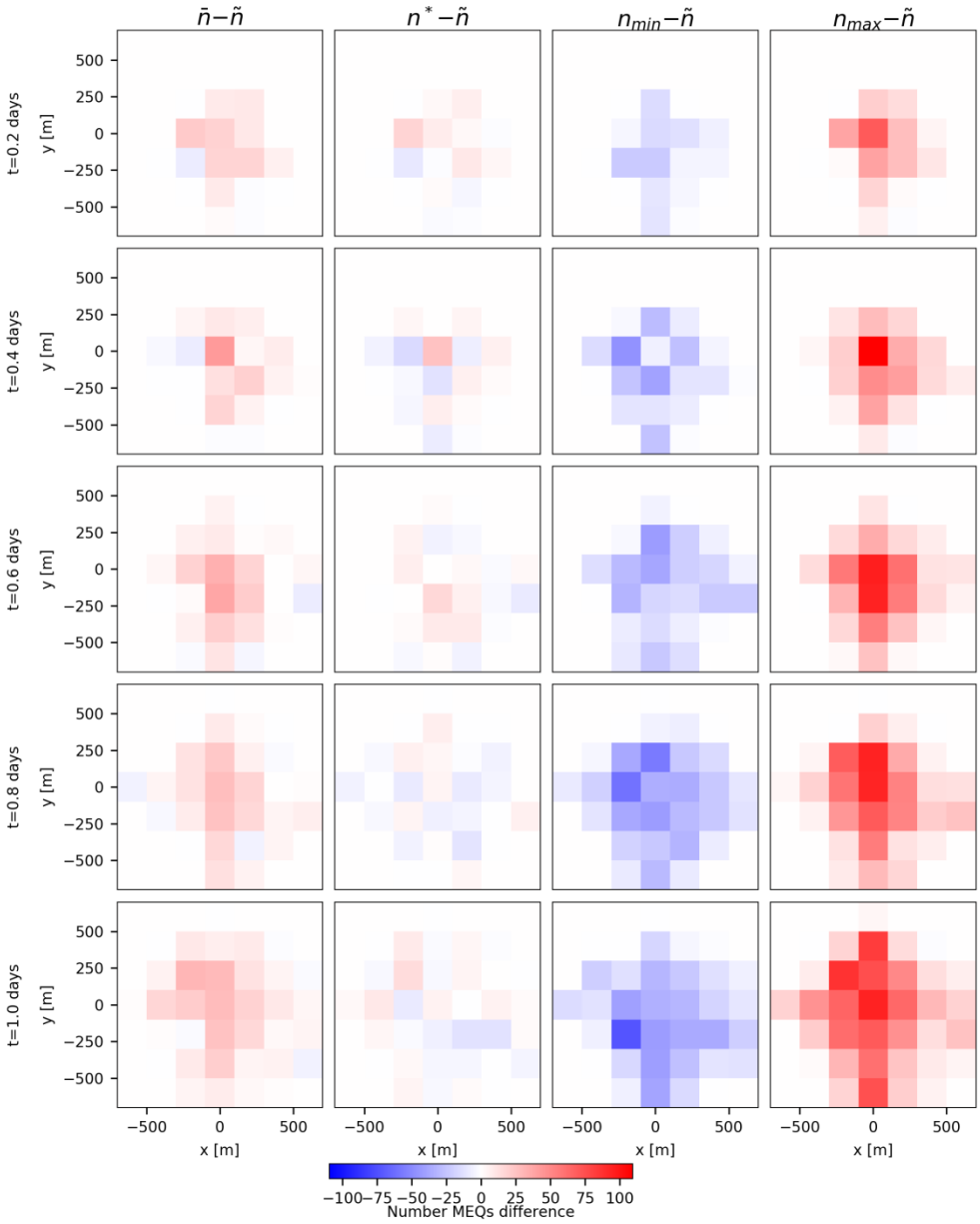

Figure 6: Difference with observed seismicity at each node at five different times for four different datasets: true seismicity, best fit, minimum values, maximum values

Thus, while $\bar{\boldsymbol{\Omega}}$ is not included in the ensemble [**Ω**], the permeability evolution scenario it describes for most of the simulation duration is. However, the inclusion of $\bar{\boldsymbol{\Omega}}$ is a necessary but not sufficient condition to affirm that the ensemble of parameters, [**Ω**] is complete, as we cannot discard the existence of other regimes fitting the observations missed by the inversion.

While permeability models for each node are remarkably well constrained from 0 days to 0.75 days, this is not the case for the permeability distribution at t=1 day (Figure 7). This is because of the inertia between permeability changes and pressure response (and subsequent seismicity). As we do not model pressure and hypocenter density changes after t=1 day, there is no information available to the inversion process to constrain permeability at this time, hence permeability estimation for the final time contains greater error.

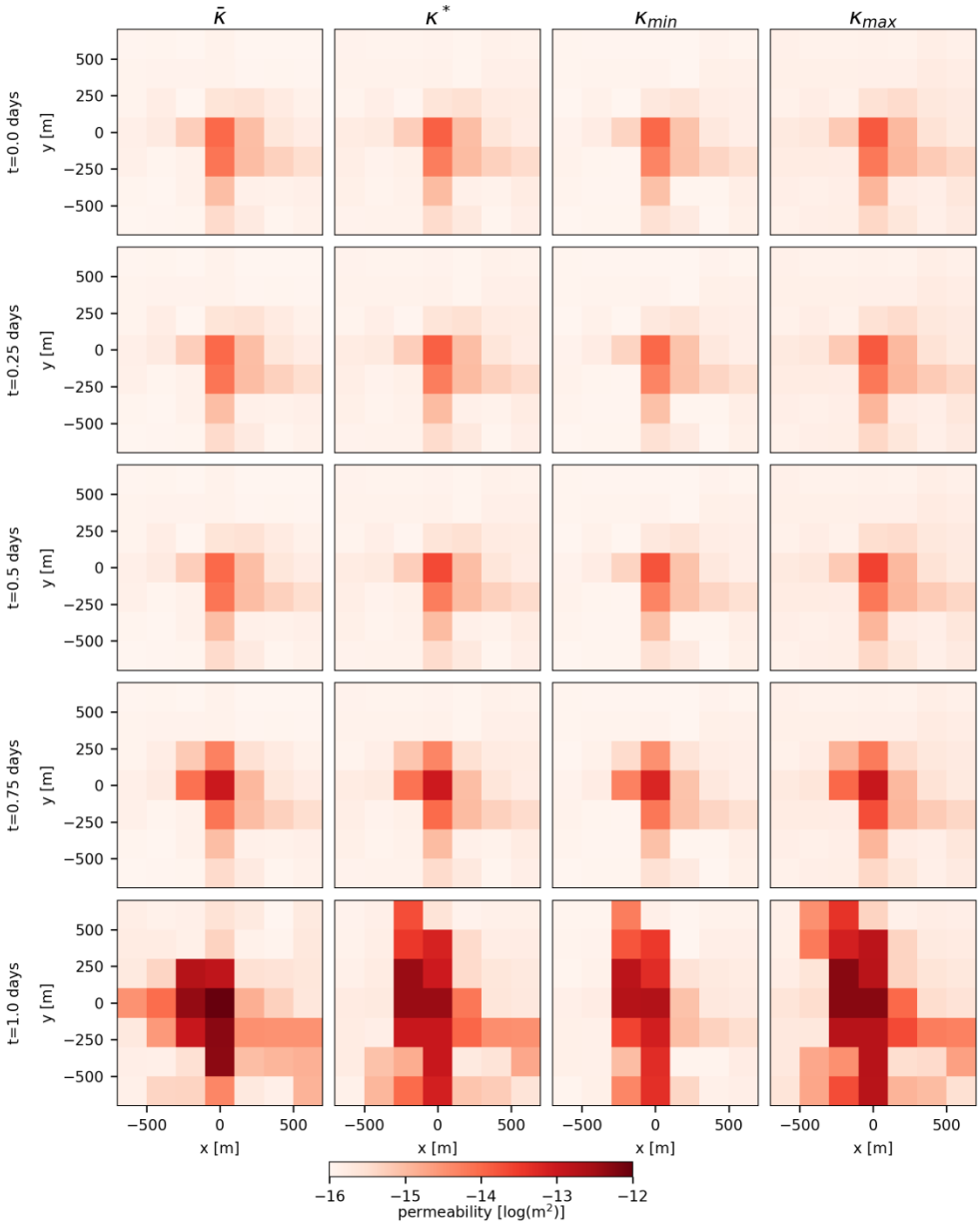

Figure 7: Permeability spatial distribution at five different times for four different datasets: synthetic data, best fit, minimum values, maximum values

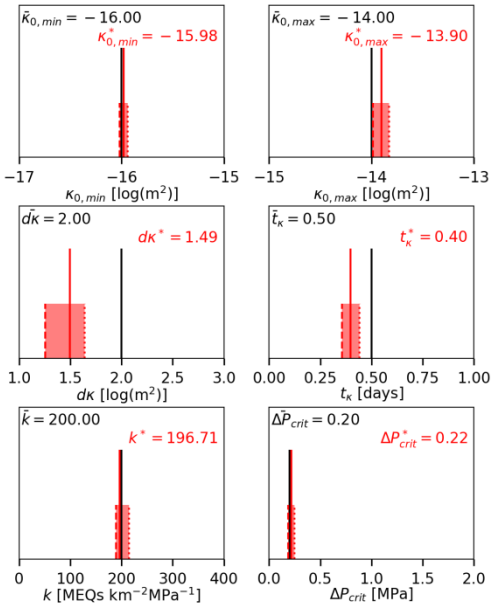

Figure 8: Distribution of inverted parameters compared to the true values

5. CONCLUSIONS

In this paper, we have presented a new method to obtain the permeability enhancement distribution from an induced seismicity cloud. The use of a synthetic data set provides a first validation of the method's potential, as well as some insight into its limitations.

A permeability distribution was successfully inverted except for the last time steps of the simulation. This is because of the inertia between permeability increase and pore pressure response. For future applications, this means that post-stimulation induced events should be included to invert with more accuracy permeability changes happening at the end of the injection phase.

Because of the uncertainties engendered by the aleatoric component of earthquakes, as well as in the localization process, the hypocenter density distribution observed is different from the one exactly reflecting permeability changes. This means that the best fitted model is different from the real dataset and a large subset of parameters producing a "good-enough" match is thus more interesting than the best-fit model. Quantifying uncertainties can help set the criterion to select the range of those models.

The objective with such algorithm that produces a range of possible scenarios instead of the absolute minimum is to obtain the complete set of parameters combination satisfying a goodness of fit criteria. Because of the large number of parameters, completeness of the parameter distribution was not achieved even with a simple synthetic problem. However, when looking at the produced permeability distributions, a single permeability enhancement regime was identified, which contains the true scenario (except for the final time steps of the simulation as explained before). Thus, the inversion is reasonably successful.

The inversion process is much easier when the functional form of the permeability assignment model is assumed to be known. In this problem, we artificially eliminated structural error, and considered only observation error. To use our method on real datasets, as for example the 2003 Habanero stimulation, we should consider greater flexibility in our permeability model to avoid such structural error jeopardizing the quality of the inversion. However, completeness in the permeability assignment model is inherently unobtainable, as this would require an infinite number of parameters, and we could never discard the possibility that structural error is not influencing our results. Therefore, there will always be a balance between the efficiency of the inversion and the range of permeability enhancement regimes considered.

The use of this method with real datasets will give insight into the reservoir development process in EGS stimulation and the extent of the engineered reservoir. It could potentially shed light on the primary driving mechanisms responsible for permeability development. In Habanero, there are two suspects: hydroshearing and thermal effects. Both reactivate existing cracks through the reduction of the effective stress, hydroshearing through pressure increase, thermal effects through rock cooling. Because pressure and temperature are modelled, if we obtain a picture of the permeability development regime, we can quantify how it couples with each of those variables, and weigh the dominance of each mechanism against the other.

AKNOWLEDGEMENTS

This work was funded by the Center for Space and Earth Science at Los Alamos National Laboratory.

REFERENCES

Dempsey, D., Barton, C. and Catalinac, A.: Density of Induced Earthquake Hypocenters as a Proxy for Pore Pressure Increase during Well Stimulation, *Proceedings,* 50th US Rock Mechanics/Geomechanics Symposium, American Rock Mechanics Association (2016).

Baisch, S., Weidler, R., Vörös, R., Wyborn, D. and de Graaf, L.: Induced seismicity during the stimulation of a geothermal HFR reservoir in the Cooper Basin, Australia, *Bulletin of the Seismological Society of America*, **96**(6), (2006), 2242-2256.

Langenbruch, C., Dinske, C. and Shapiro, S.A.: Inter event times of fluid induced earthquakes suggest their Poisson nature, *Geophysical Research Letters*, **38**(21), (2011).

Pearson, C.: The relationship between microseismicity and high pore pressures during hydraulic stimulation experiments in low permeability granitic rocks, *Journal of Geophysical Research: Solid Earth*, **86**(B9), (1981), 7855-7864.

Riffault, J., Karra, S., Archer, R. and Dempsey, D.: Microseismicity cloud can be substantially larger than the associated stimulated fracture volume: the case of the Paralana Enhanced Geothermal System, *Journal of Geophysical Research: Solid Earth*, (*submitted*).

Schmitt, L.M.: Theory of genetic algorithms, *Theoretical Computer Science*, **259**(1-2), (2001), 1-61.

Shapiro, S.A., Rentsch, S. and Rothert, E.: Characterization of hydraulic properties of rocks using probability of fluid-induced microearthquakes, *Geophysics*, **70**(2), (2005), F27-F33.

Tarrahi, M. and Jafarpour, B.: Inference of permeability distribution from injection-induced discrete microseismic events with kernel density estimation and ensemble Kalman filter, *Water Resources Research*, **48**(10), (2012).

Weidler, R., Gérard, A., Baria, R., Baumgärtner, J. and Jung, R.: Hydraulic and micro-seismic results of a massive stimulation test at 5 km depth at the European Hot-Dry-Rock test site, Soultz, France, *Proceedings*, 27th Workshop on Geothermal Reservoir Engineering, Stanford University, Stanford, CA (2002).

Zyvoloski, G.: FEHM: A control volume finite element code for simulating sub-surface multi-phase multi-fluid heat and mass transfer, *Los Alamos Unclassified Report*, (2007), LAUR-07-3359.